The Mg^{2+} Requirements for Rho Transcription Termination Factor: Catalysis and Bicyclomycin Inhibition†

Thomas P. Weber,‡ William R. Widger,*,§ and Harold Kohn*,||

Department of Chemistry and Department of Biology and Biochemistry, University of Houston, Houston, Texas 77204, and Division of Medicinal Chemistry and Natural Products, School of Pharmacy, University of North Carolina, Chapel Hill, North Carolina 27599

Received June 17, 2002; Revised Manuscript Received August 14, 2002

ABSTRACT: Kinetic studies document that the essential *Escherichia coli* transcription termination factor rho utilizes Mg^{2+} and ATP as a substrate and requires a second Mg^{2+} ion for maximum poly(C)-dependent ATP hydrolysis activity. The velocity curves show a classic nonessential Mg^{2+} activation pattern in which Mg^{2+} augments hydrolysis by 39% and gives a K_1' for MgATP of 9.5 μM in the presence of excess Mg^{2+} and a K_1 for MgATP of 21.2 μM under limiting Mg^{2+} concentrations. Bicyclomycin (**1**), a commercial antibiotic that inhibits rho, weakened Mg^{2+} binding at the nonessential site and disrupted the nonessential Mg^{2+} activation pathway for poly(C)-dependent ATP hydrolysis. The K_i values for **1** were 23 μM and 35 μM under excess and limiting Mg^{2+} conditions, respectively, while the $K_{Mg(app)}$ for nonessential Mg^{2+} increased with increasing **1** concentrations. These findings, when combined with reported mechanistic studies, provide an emerging picture of key catalytic and substrate binding sites that are necessary for rho function and that are proximal to the **1** binding site.

The essential *Escherichia coli* rho factor (*1*) terminates select transcripts at the ends of genes and operons (*2*) and at regulatory points before and between genes (*3*). Rho is an RNA-binding protein that belongs to a family of helicases with a homohexameric structure shaped like a toroid (*4a*). The monomers are identical, consisting of 419 amino acid residues divided into two structural domains: the primary RNA-binding domain (residues 1−151) and the ATP[1] hydrolysis domain (residues 167−419) (*5*). A solution structure of the N-terminal 130 residues of rho has been solved using NMR techniques (*6*), and a crystal structure is also available (*7*). Structural information of the intact protein is lacking since hexameric rho has resisted crystallization. However, rho factor shows considerable sequence and predicted secondary structure similarity to the β-subunit of F_1-ATP synthase (*8*), and models of rho based on this structure have been presented (*8*−*12*). We observed a nearly perfect alignment of the predicted secondary structure of rho after residue 160, which included specific residues involved in ATP binding and catalysis (*11*, *12*).

Rho binds to specific cytidine-rich areas of newly synthesized RNA at the primary RNA-binding site and makes advancing contacts with the transcript at the secondary RNA-binding site in a process fueled by nucleoside triphosphate hydrolysis (*4*). A tethered tracking mechanism that results in disruption of the RNA polymerase−transcription complex, transcription termination, and the release of RNA and rho has been proposed for rho translocation (*4*).

The macromolecular target for the commercial antibiotic bicyclomycin (**1**) is rho (*13*). Mechanistic studies indicate that bicyclomycin interferes with rho RNA tracking and prevents protein conformational changes necessary for ATP hydrolysis (*14*). Bicyclomycin is projected to bind to a protein cleft in rho that is positioned at the interface of two rho subunits and close to the ATP binding and RNA tracking sites (*15*).

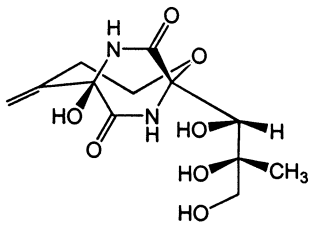

1

The sequence similarity between rho and F_1-ATP synthase prompts the question: do these proteins share an equivalent enzyme mechanism? F_1F_o-ATP synthase catalyzes the conversion of ADP and P_i to ATP where ATP synthesis occurs in nucleotide binding sites located in the F_1 sector (*16*). Detachment of the membrane-embedded F_o protein to give F_1-ATP synthase reverses the catalytic process permitting ATP hydrolysis. F_1-ATP synthase is characterized by three catalytic MgATP sites that sequentially hydrolyze ATP and three sites that are noncatalytic. MgATP is also the suggested

† This work was supported by National Institutes of Health Grant GM37934 and Robert A. Welch Foundation Grant E1381 (W.R.W.).

* To whom correspondence should be addressed. W.R.W.: e-mail, widger@uh.edu. H.K.: e-mail, harold_kohn@unc.edu.

‡ Department of Chemistry, University of Houston.

§ Department of Biology and Biochemistry, University of Houston.

|| University of North Carolina.

[1] Abbreviations: ATP, adenosine 5′-triphosphate; DTT, dithiothreitol; EDTA, ethylenediaminetetraacetic acid; PEI-TLC, poly(ethylenimine) thin-layer chromatography; SDS−PAGE, sodium dodecyl sulfate−polyacrylamide gel electrophoresis; TE, Tris-HCl and EDTA; Tris, tris(hydroxymethyl)aminomethane.

10.1021/bi020420w CCC: $22.00 © 2002 American Chemical Society
Published on Web 10/08/2002

substrate for rho function (*17*). Without Mg^{2+} there is no ATP hydrolysis and no transcription termination (*17c*, *18a*). Little is known about the molecular pathway for rho ATP hydrolysis, and only a few reports have appeared on the role of Mg^{2+} in rho-mediated processes (*4a*, *18*).

We report herein the Mg^{2+} requirements for rho-mediated poly(C)-dependent ATP hydrolysis. We show that maximal ATPase activity requires a *second* Mg^{2+} ion and further demonstrate that bicyclomycin binding inhibits the catalytic role provided by this second Mg^{2+} ion.

MATERIALS AND METHODS

Materials. Bicyclomycin was provided as a gift from Fujisawa Pharmaceutical Co., Ltd., and was purified by three successive silica gel chromatographies using 20% methanol−chloroform as the eluant. [γ-^{32}P]ATP (6000 Ci/mmol) was purchased from Perkin-Elmer (Boston, MA), Bio-Spin 6 columns were from Bio-Rad (Hercules, CA), and PEI-TLC plates used for ATPase assays were obtained from J. T. Baker, Inc. (Phillipsburg, NJ). Poly(C) was from Sigma (St. Louis, MO) and was dissolved in 100 μL of TE buffer and dialyzed against aqueous 1.0 M potassium phosphate, pH 7.0 (8 h, 2×, 4 °C) using Slide-A-Lyzer cassettes from Pierce (Rockford, IL). All other chemicals were of reagent grade.

Bacterial Strains and Plasmids. Wild-type rho from *E. coli* was purified as described by Mott (*19*) from strain AR120 containing plasmid p39-ASE (*20*). Rho purity was determined by SDS−PAGE, and protein concentration was measured according to the Lowry assay (*21*).

Trp t′ RNA Preparation and Isolation. The DNA substrate was a truncated form of the *trp* operon (*22*) modified and placed in the pTRP5 plasmid as described (*14*).

Trp t′ RNA was made using *Sal*I-linearized pTRP5 plasmid and T7 RNA polymerase. The reaction (100 μL) was carried out in transcription buffer (40 mM Tris·HCl, 15 mM $MgCl_2$, 5 mM DTT, and 0.5 mg/mL acetylated BSA) containing 1 mM ATP, GTP, and UTP, 24 μM CTP, 40 units of RNase inhibitor, and 25 μg of DNA. The reaction was started with 1.4 μg of T7 RNA polymerase and was incubated at 42 °C for 2 h, another 0.56 μg of enzyme was added, and the reaction was incubated for another 2 h. RNase-free DNase (1 μL) was added, and the RNA was purified using an RNeasy kit (Qiagen, Inc., Santa Clarita, CA). EDTA was added to a final concentration of 40 mM, and the *trp t′* RNA was dialyzed against 100 mM potassium phosphate, pH 7.0 (6 h, 1×, 4 °C), and 50 mM Tris·HCl, pH 7.9 (8 h, 2×, 4 °C). Purity was determined by urea−PAGE, and the RNA concentration was determined by UV at A_{260} using an extinction coefficient of 4.5 μM^{-1} cm^{-1}.

Spin Column Purification. Rho (10 μM) in an aqueous 40 mM Tris·HCl (pH 7.9) solution containing EDTA (20 mM) was incubated on ice (10 min). Aliquots (100 μL) of the protein solution were applied to Bio-Spin 6 columns, which were pretreated (2×) with 500 μL of an aqueous 40 mM Tris·HCl (pH 7.9) solution containing 50 mM KCl and then centrifuged (2000 rpm, 4 °C, 2 min). Measurements of the spin column-treated rho showed no loss of protein (Lowry) and a residual activity of 10% or less in Mg^{2+}-free buffer [poly(C)-dependent ATPase assay].

Poly(C)-Dependent ATPase Assay (23). The ribonucleotide-stimulated ATPase activity of rho at 32 °C was assayed by measuring the amount of ^{32}P-labeled inorganic phosphate hydrolyzed from ATP after separation on PEI-TLC plates (prerun with water and dried) using 0.75 M potassium phosphate (pH 3.5) as the mobile phase (*24*). Reactions were initiated by adding ATP (varying concentrations) and 0.5 μCi of [γ-^{32}P]ATP to the solution containing 40 mM Tris·HCl (pH 7.9), 50 mM KCl, 100 nM poly(C), 40 nM rho (monomer) and $MgCl_2$ (various concentrations). The TLC plates were exposed to PhophorImager plates (Fuji and Molecular Dynamics) (3 h), scanned on a Storm 860 PC PhosphorImager, and analyzed using Molecular Dynamic's ImageQuant 5.0. The initial rates of the reactions were determined by plotting the amount of ATP hydrolyzed against time. Each reaction was performed in duplicate, and the results were averaged.

Trp t′-Dependent ATPase Assay. The *trp t′*-stimulated ATPase activity of rho at 45 °C was assayed using the preceding procedure. Reactions were initiated by the addition of ATP (varying concentrations) and 0.5 μCi of [γ-^{32}P]ATP to a solution containing 40 mM Tris·HCl (pH 7.9), 50 mM KCl, 65 nM *trp t′* RNA, 50 nM rho (monomer), $MgCl_2$ (varying concentrations), and 10% (v/v) DMSO.

Kinetics of Poly(C)-Stimulated Rho Activation and Inhibition by Bicyclomycin. ATPase assays were carried out as described in the preceding section using a six-channel, multiwell procedure. The reactions (100 μL) were run with 2, 4, 5, 8, 10, 16, 20, 32, 40, 64, 80, 128, 160, 256, 320, 512, 640, 1048, 1280, and 2560 μM ATP and 4, 8, 16, 32, 64, 128, 256, and 2560 μM $MgCl_2$. Each series was repeated in the presence of 15, 30, and 60 μM bicyclomycin. Samples were preincubated at 32 °C for 2 min prior to ATP addition, and five 1.4 μL aliquots were spotted onto PEI-TLC plates after 15 s and then at selected times (10−300 s) depending on the ATP concentrations.

Kinetics of trp t′-Stimulated Rho Activation. ATPase assays were carried out as described in the preceding section using a six-channel, multiwell procedure. The reactions (40 μL) were run with 8, 16, 32, 64, 128, 160, 256, 320, 512, 640, 1024, and 2560 μM ATP and 32, 64, and 256 μM $MgCl_2$. Samples were preincubated at 45 °C for 2 min before ATP was added, and five 1.4 μL aliquots were spotted onto PEI-TLC plates after 15 s and then at selected times (10−300 s) depending on the ATP concentrations.

Isothermal Titration Calorimetry Measurements. The experiments were performed at 26 °C in a MicroCal (Northampton, MA) VP ultrasensitive isothermal titration calorimeter. An aqueous solution containing 50 mM Tris·HCl (pH 7.9) and **1** (20 mM) was added to a 1.4 mL sample cell. Aliquots (55 × 5 μL) containing 300 mM $MgCl_2$ in 50 mM Tris·HCl (pH 7.9) were injected over a 10 s period, and the heat of reaction (microcalories per second) over a 3.5 min interval was determined by integration of the peak areas using Origin software from MicroCal. Binding was complete within the first third of the titration, and the heat of dilution was determined from the baseline once titration was complete. The Origin software provided the best-fit values of $\Delta H°$, the stoichiometry of binding (n), and the dissociation constant (K_d) from plots of heat evolved per mole of $MgCl_2$ injected versus the $MgCl_2$/**1** molar ratio (*24*).

Table 1: Rho-Mediated Poly(C)-Dependent ATPase Activity at Near Constant MgATP Concentrations

$[Mg_{tot}]$ (μM)	$[ATP_{tot}]$ (μM)	[MgATP][a] (μM)	$[Mg_{free}]$ (μM)	$[ATP_{free}]$ (μM)	V^b (μmol min^{-1} mg^{-1})
32	320	26.6	5.4	293.4	10.5 ± 0.01
80	80	34.5	45.5	45.5	12.7 ± 0.5
400	40	34.4	365.6	5.6	15.6 ± 1.6

[a] Initial MgATP concentrations were calculated using a K_d(MgATP) = 60 μM (*28*). [b] The values are the average of two determinations.

Chart 1: Kinetic Model of ATP Hydrolysis in Rho[a]

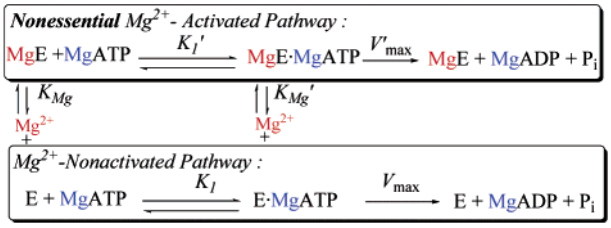

[a] MgATP binds to the catalytic site, and free Mg^{2+} is a nonessential activator.

RESULTS

Rho protein was prepared as previously described (*19*) from the *E. coli* strain AR120 containing the overexpression plasmid p39-ASE and extensively dialyzed against buffer containing 0.1 mM EDTA. This preparation showed residual ATPase activity (*23*) of 35% in Mg^{2+}-free buffer compared with 10 mM $MgCl_2$ buffer (*25*). When rho in ATPase buffer (*25*) containing EDTA (20 mM) was passed through a Bio-Spin 6 spin column (Bio-Rad, Hercules, CA), the activity was reduced to 10% of fully activated protein. However, when 10 mM Mg^{2+} was added, the ability to be 90% activated was regained. These findings indicated that a low level of Mg^{2+} or other ions bound tightly to rho.

Adding varying concentrations of Mg^{2+} and ATP (5′-ATP-Na_2) to the purified rho showed that ATP hydrolysis in the poly(C)-dependent assay did not depend solely on MgATP concentrations and that free Mg^{2+} augmented the conversion of ATP to ADP and P_i when the MgATP concentration was held at a near constant value (Table 1). This finding suggested that Mg^2 served as a nonessential activator (*26*) (Chart 1).

To document the nonessential Mg^{2+} activation pathway, we monitored the ATP hydrolysis at different Mg^{2+} concentrations (4, 8, 16, 32, 64, 128, 256, 2560 μM) and at different ATP concentrations (2, 4, 5, 8, 10, 16, 20, 32, 40, 64, 80, 128, 160, 256, 320, 512, 640, 1048, 1280, 2560 μM) (Figure 1A). The 160 reaction matrix was run in duplicate, and the average rates were plotted against ATP concentrations for the various Mg^{2+} concentrations (Figure 1A). The experimental design provided conditions under which the Mg^{2+} concentrations exceeded that of ATP, and the ATP concentrations were greater than Mg^{2+}. Specifically, we observed a steady increase in the V_{max} for the reaction rates with increasing Mg^{2+} concentrations, an elevated hydrolysis rate at low ATP concentrations (128−320 μM) for Mg^{2+} concentrations between 4 and 256 μM that decreased at higher ATP concentrations (512−2560 μM), and the appearance of near hyperbolic velocity hydrolysis curves with high Mg^{2+} concentrations (2560 μM). Figure 1A inset shows

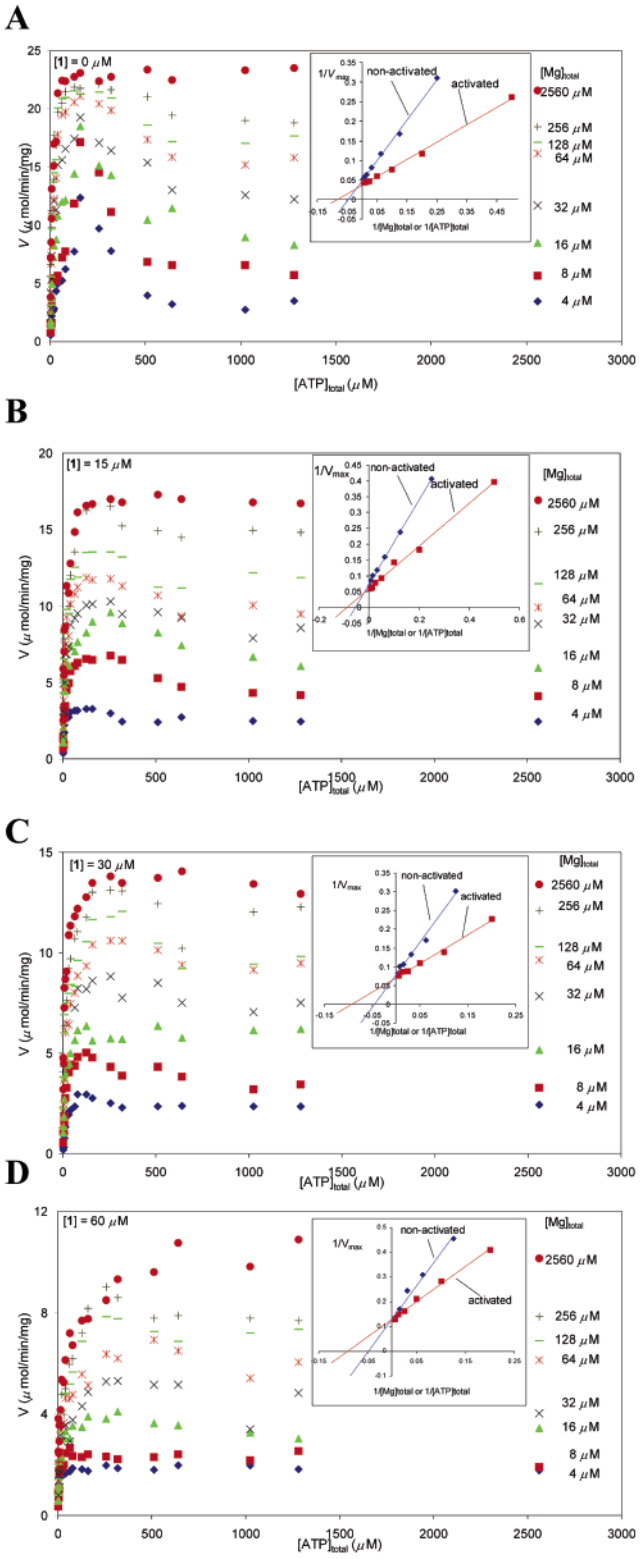

FIGURE 1: Velocity curves in poly(C)-dependent ATPase assay of rho *vs* total ATP concentration at various fixed Mg^{2+} concentrations. The reactions were conducted using a solution (100 μL) containing ATPase buffer, rho [40 nM (monomer)], poly(C) (100 nM), and various concentrations of ATP and Mg^{2+} at 32 °C. The average velocities of two determinations are plotted. Inset: double reciprocal plot of the poly(C)-dependent ATPase activity of rho protein with either varying ATP (Mg^{2+} activated) or Mg^{2+} (Mg^{2+} nonactivated) concentrations. Panels: (A) **1** = 0 μM, (B) **1** = 15 μM, (C) **1** = 30 μM, and (D) **1** = 60 μM.

Table 2: Key Thermodynamic and Kinetic Parameters for Poly(C)-Dependent ATP Hydrolysis in the Presence of **1**

[**1**] (μM)	K_1 (μM)	K_1' (μM)	$K_{Mg(app)}$ (μM)	$V_{max(app)}$[a] (μmol min^{-1} mg^{-1})	$V'_{max(app)}$[a] (μmol min^{-1} mg^{-1})	V_{max}/V'_{max}
0	21.2	9.5	12.9	20.0	27.8	0.72
15	19.4	11.4	17.5	13.5	16.9	0.80
30	22.2	10.7	95.2	12.8	14.1	0.91
60	20.3	10.8	135	7.7	7.8	0.99

[a] The values are the average of two determinations.

the double reciprocal plot of 1/(rate of ATPase activity) versus 1/[ATP]$_{total}$ for reactions performed in the presence of excess Mg^{2+} (Mg^{2+} activated; [Mg^{2+}] = 256 and 2560 μM, [ATP] = 2−256 μM) and a similar plot of 1/(rate of ATPase activity) versus 1/[Mg^{2+}]$_{total}$ for reactions run at high ATP concentrations (Mg^{2+} nonactivated; [Mg^{2+}] = 4−256 μM, [ATP] = 1280 and 2560 μM) (*26a*). Extrapolation of the data points from the double reciprocal plot to the *y*-axis provided the V'_{max} (Mg^{2+} activated) and V_{max} (Mg^{2+} nonactivated). Correspondingly, when the data points were extended to the *x*-axis, we obtained the Briggs−Haldane constants K_1' (Mg^{2+} activated) and K_1 (Mg^{2+} nonactivated). We found that, in the presence of excess Mg^{2+}, the K_1' for MgATP was 9.5 μM (*27*) and the V'_{max} was 27.8 μmol min^{-1} mg^{-1} and that, under limiting Mg^{2+} conditions, the corresponding constant K_1 for MgATP was 21.2 μM and the V_{max} was 20.0 μmol min^{-1} mg^{-1} (Chart 1, Table 2). These findings indicate that, under conditions when excess Mg^{2+} exists in solution [K_d(MgATP) = 60 μM (*28*)], Mg^{2+} enhanced the ATP hydrolysis rate by 39%. The dissociation constant for Mg^{2+} binding to the rho nonessential Mg^{2+} binding site, K_{Mg}, was calculated using the rate equation (eq 1) corresponding to the kinetic scheme (Chart 1) (*26a*). We determined that K_{Mg} (12.9 μM) was comparable with K_1' and K_1 (9.5−21.2 μM) in the absence of **1**.

The experimental data in Figure 1A were simulated using eq 1. We employed a nonlinear regression program (SigmaPlot 2001), and the parameters (V_{max}, V'_{max}, K_1, K_1', $K_{Mg(app)}$, K_0) were set to the graphically determined values, allowing a 15% variation except for the total metal concentration. Satisfactory plots were obtained for Mg^{2+} concentrations from 16 to 250 μM (Supporting Information). At Mg^{2+} concentrations lower than 16 μM the calculated velocities were lower than the experimentally observed values at ATP concentrations less than 256 μM, which suggests that trace levels of metals in rho contributed to the observed ATP hydrolysis rates.

When we repeated this experiment at different **1** concentrations (15, 30, 60 μM), we saw a steady decrease in the ATP hydrolysis rate and a *rapid* loss of the elevated rates for ATP hydrolysis at low-to-moderate Mg^{2+} concentrations (4−256 μM) (Figure 1B−D). Panels A and B of Figure 2 show the double reciprocal plots for the 0−60 μM **1** reactions in the presence of excess Mg^{2+} (Mg^{2+} activated) and excess ATP (Mg^{2+} nonactivated), respectively. Table 2 summarizes the thermodynamic and kinetic parameters determined from graphic analyses and shows that while the K_1' and K_1 values for MgATP remain constant as the **1** concentrations reach its I_{50} value (60−70 μM) (*13*), $V'_{max(app)}$ approached $V_{max(app)}$. Significantly, when increasing amounts of **1** (0, 15, 30, 60 μM) were added, the apparent dissociation constant for

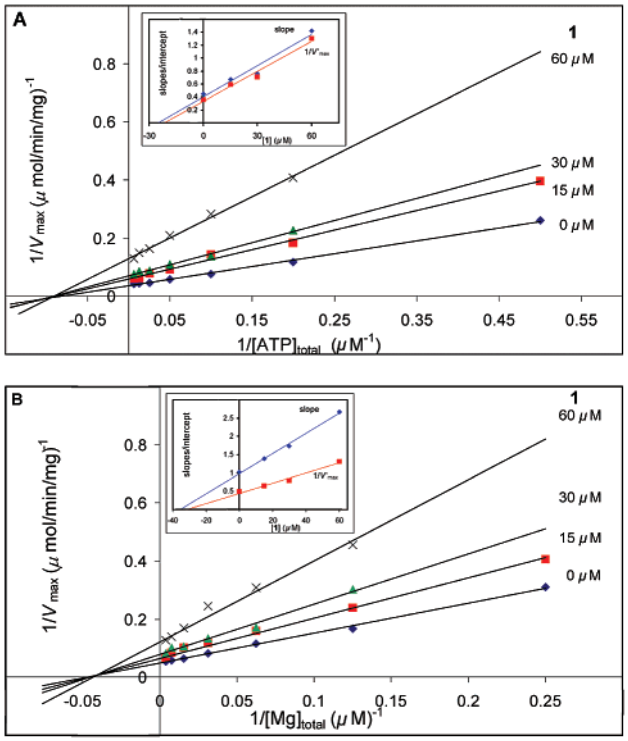

FIGURE 2: Effect of **1** on rho-mediated poly(C)-dependent ATPase activity: (A) excess Mg^{2+} employed; (B) excess ATP employed. See legend to Figure 1 for reaction conditions. Insets: plots of the slopes and intercepts versus **1** concentration.

nonessential Mg^{2+} binding to rho, $K_{Mg(app)}$, progressively increased from 12.9 to 135 μM (Table 2), indicating that the antibiotic weakened the protein interaction for the second, nonessential Mg^{2+} site. When the intercepts and slopes obtained in Figure 2 were plotted against **1** concentrations (Figure 2 insets), a linear response resulted, providing **1** K_i values of 23 and 35 μM under excess and limiting Mg^{2+} conditions, respectively.

$$V = \frac{\frac{[MgATP]}{K_1}V_{max} + \frac{[Mg][MgATP]}{K_{Mg}K_1'}V'_{max}}{1 + \frac{[Mg]}{K_{Mg}} + \frac{[MgATP]}{K_1} + \frac{[Mg][MgATP]}{K_{Mg}K_1'}} \quad (1)$$

or in terms of [Mg]$_{total}$ and [ATP]$_{total}$ replace

$$[MgATP] = \frac{[Mg]_{total} + [ATP]_{total} + K_o}{2} - \left\{\left(\frac{[Mg]_{total} + [ATP]_{total} + K_o}{2}\right)^2 - [Mg]_{total}[ATP]_{total}\right\}^{1/2}$$

$$[Mg] = [Mg]_{total} - \frac{[Mg]_{total} + [ATP]_{total} + K_o}{2} - \left\{\left(\frac{[Mg]_{total} + [ATP]_{total} + K_o}{2}\right)^2 - [Mg]_{total}[ATP]_{total}\right\}^{1/2}$$

where $K_o = K_d$(MgATP).

We examined three aspects of the proposed ATP hydrolysis pathway (Chart 1). First, we determined if the observed loss in rho poly(C)-dependent ATPase activity with increasing levels of ATP may have resulted from MgATP displacement by ATP. Rho solutions were prepared in which the

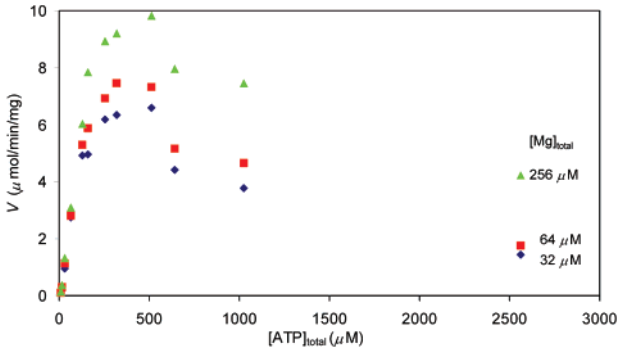

FIGURE 3: Velocity curves of rho in *trp t′*-dependent ATPase assay *vs* total ATP concentration at various fixed Mg^{2+} concentrations. The reactions were conducted using a solution (40 μL) containing ATPase buffer, rho [50 nM (monomer)], and *trp t′* (65 nM) at various concentrations of ATP and Mg^{2+} at 45 °C in 10% (v/v) DMSO.

effective MgATP concentration was held at 400 μM and the ATP concentration ranged from 400 to 4000 μM. We observed no significant difference in rho poly(C)-dependent activity despite the 10-fold change in ATP concentration (data not shown). This finding was in agreement with an earlier report by Stitt that ATP did not bind to rho in either the presence or absence of poly(C) (*17c*).

We then asked if the nonessential Mg^{2+}-activated pattern for rho-dependent ATP hydrolysis with poly(C) (Figure 1A) was observed for physiologically relevant RNA. Platt and co-workers have reported differences in the Mg^{2+} dependence of ATPase activation with poly(C) compared with natural RNA cofactors (*18c*). We chose *trp t′*, RNA previously shown to have a rho-dependent termination site (*22*), and conducted an abbreviated experiment corresponding to Figure 1A because of the limited quantities of this RNA. We determined the rates of ATP hydrolysis when Mg^{2+} was held at 32, 64, and 256 μM and ATP ranged from 0 to 2560 μM (Figure 3). We found that using our normal conditions [10 mM $MgCl_2$, aqueous Tris·HCl buffer (pH 7.9), 32 °C] *trp t′* afforded ATPase hydrolysis rates less than 5% of those observed with poly(C). When we ran the *trp t′* experiments in aqueous Tris·HCl buffered solutions (pH 7.9) containing 0.5 mM $MgCl_2$ and 10% DMSO (v/v) and at 45 °C, we obtained ATP hydrolysis rates that were approximately 65% of those obtained for poly(C)-dependent processes run under the same conditions (data not shown). Richardson and Macy have shown that DMSO and higher temperatures destabilize the secondary structure of RNA permitting rho binding and enhancing ATP hydrolysis (*29*). Using these conditions for the *trp t′* RNA, we observed the hallmarks of nonessential Mg^{2+} activation kinetics: high V_{max} under excess Mg^{2+} conditions and low ATP concentrations (Mg^{2+} activated) and significantly lower V_{max} values when Mg^{2+} was limiting and the ATP concentrations were high (Mg^{2+} nonactivated).

Finally, we determined if the observed increase in the dissociation constant $K_{Mg(app)}$ for the rho−Mg^{2+} complex when bicyclomycin was added stemmed, in part, from Mg^{2+} binding to **1**. Accordingly, we measured the binding isotherms after $MgCl_2$ addition (0−3 equiv) to aqueous 50 mM Tris·HCl (pH 7.9) buffered solutions containing **1**. We measured low levels of reaction heat when 1 mM **1** solutions were used. Elevating the **1** concentration to 20 mM led to detectable levels of heat, and best-fit analysis gave a binding isotherm for a 1:1 Mg·**1** complex with a $K_d = 5$ mM. Thus, the putative Mg·**1** complex is ~80-fold weaker than the MgATP complex ($K_d = 60$ μM) (*28*). Similarly, we estimate that the Mg·**1** species is ~400-fold weaker than the Mg·rho complex ($K_{Mg(app)} = 12.9$ μM; Table 2).

DISCUSSION

Previous studies showed that rho retained significant poly(C)-dependent ATP hydrolysis activity without $MgCl_2$ and that hydrolysis is prevented by adding EDTA to the reaction solution (*17c*, *18a*). We demonstrated that the use of spin columns and EDTA-pretreated rho provided a rapid method for removing low levels of divalent metal ions from purified rho solutions. The rho protein showed residual poly(C)-dependent ATPase activity (10%), indicating that trace levels of divalent metals remained. Repetition of the spin column procedure did not reduce the level of ATPase activity. These findings were reminiscent of the earlier report by Lowery and Richardson showing that extensive dialysis of rho against EDTA-containing buffers still retained residual ATPase activity (*18a*) and studies by Senior and co-workers demonstrating that purified bovine F_1-ATP synthase retained a tightly bound Mg^{2+} (estimated $K_d < 10^{-11}$ M) (*30*).

Our kinetic studies revealed that a second Mg^{2+} facilitated ATP conversion to ADP and P_i and that it was necessary for maximal activity in the poly(C)-dependent assay (Figure 1A). The nonessential Mg^{2+}-activated pathway (Chart 1) accelerated ATP hydrolysis by 39%. Enhanced rho-dependent ATPase activity is likely to increase transcription termination efficiencies at prescribed RNA sequences. Indeed, we observed nonessential Mg^{2+} kinetic activation of ATP hydrolysis with *trp t′* RNA (*22*) (Figure 3).

How does the nonessential Mg^{2+} catalyze ATP hydrolysis? There are several possibilities. The nonessential Mg^{2+} may facilitate ATP cleavage to ADP and P_i, enhance MgATP binding, chaperon MgATP to the nucleotide binding site, and assist in ADP removal. The kinetic data are compatible with each of these pathways. Clues concerning the role of the nonessential Mg^{2+} come from the inhibitory effect of **1** on this process (Figure 1B−D). We observed that addition of **1** led to the complete loss of the nonessential Mg^{2+} activation and a 10-fold increase in $K_{Mg(app)}$ from 12.9 to 135 μM when the bicyclomycin concentration reached its I_{50} value. This finding indicated that 60 μM **1** fully prevented the nonessential Mg^{2+}-activated process and reduced the V'_{max} to 28% of its former value (V'_{max} without **1** = 27.8 μmol min^{-1} mg^{-1}; V'_{max} with 60 μM **1** = 7.8 μmol min^{-1} mg^{-1}). The pronounced loss of the nonessential Mg^{2+}-activated ATP hydrolysis pathway upon **1**·rho binding suggests that **1** either weakens ATP (MgATP) binding or perturbs the nonessential Mg^{2+}-assisted ATP hydrolysis pathway or both, rather than disrupting nucleotide transport.

Graphic analysis of the data provided K_i values for **1** of 23 μM and 35 μM under saturating and limiting Mg^{2+} conditions, respectively, and showed that the nonessential Mg^{2+}-activated pathway (saturating Mg^{2+} levels) was uniquely sensitive to added **1**. Disruption of the nonessential Mg^{2+} activation process led to an appreciable loss of rho-mediated poly(C)-dependent ATPase activity, and thus less **1** (23 μM) was required to inhibit total rho activity by one-half. Nonetheless, ATPase activity remained under conditions in

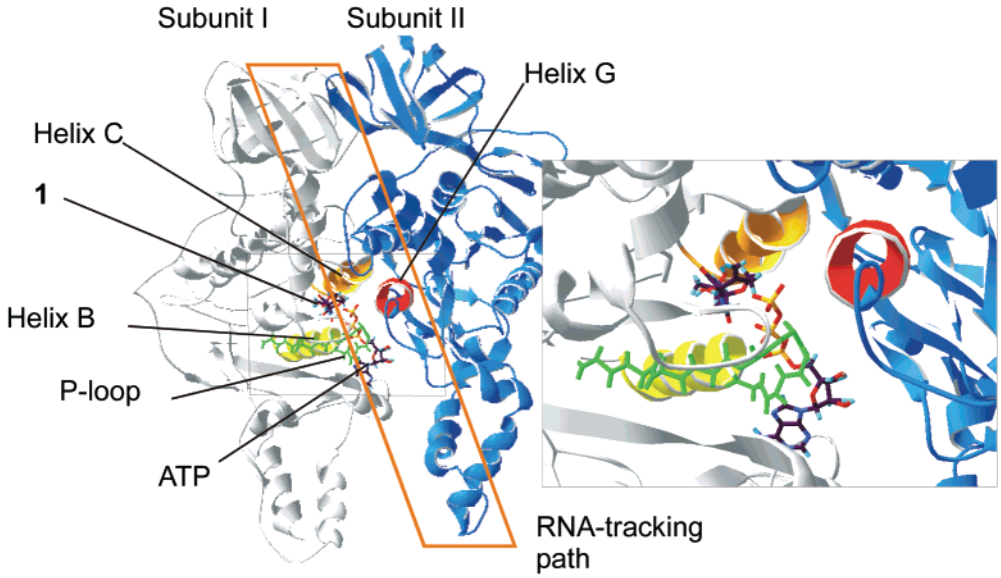

FIGURE 4: A model of the bicyclomycin binding pocket. The key helices [B (yellow) and C (brown)] for antibiotic binding, the ATP binding site, the P-loop (green backbone), and helix G (red) on the neighboring subunit are shown. The projected secondary RNA tracking site facing the central hole of rho is given in the box. Inset: a blow-up of the **1** binding pocket showing the proximity of the ATP hydrolysis site and helix G. The model was created using Swiss pdb Viewer (*31*).

which the nonessential Mg^{2+}-activated pathway does not occur (e.g., **1** = 60 μM, Figure 1D, V_{max} = 7.7 μmol min^{-1} mg^{-1}), and use of higher levels of **1** (e.g., **1** = 400 μM) led to the near total loss of poly(C)-dependent ATPase activity (*27b*). This finding indicates that the antibiotic disrupts several catalytic pathways necessary for protein function. In agreement with these results, we have shown that **1** inhibits RNA binding to the rho secondary site leading to the loss of ATPase activity (*14*).

We, and others, have reported a structural model for rho based on the sequence and predicted secondary structural similarity to the β-subunit of F_1-ATP synthase (*8*−*12*). We have positioned the bicyclomycin binding pocket to be between the rho B and C helices with the **1** C(1) triol group pointing toward the outside of rho and the C(5)−C(5a) exomethylene unit pointing toward the terminal γ-phosphate and the P-loop (residues 175−183) (Figure 4) (*15*). Positioning **1** at this site places the antibiotic at or near the catalytic ATP site, but not at the ATP binding site, and within a few angstroms of the G-helix on the neighboring subunit (residues 332−336) that forms part of the extended secondary RNA tracking site (*32*, *33*). A similar projection of the bicyclomycin binding pocket has been presented by Richardson and co-workers (*34*). Our findings that **1** inhibits the nonessential Mg^{2+}-activated pathway contribute to an emerging picture of rho (*12*) showing that the key catalytic and substrate binding sites (*12*, *15*, *33*, *35*) necessary for rho function are close to the putative **1** binding site (*12*, *15*, *34*). Current studies focus on determining the specific rho sites for Mg^{2+} binding and learning how Mg^{2+} assists ATP hydrolysis.

ACKNOWLEDGMENT

We thank Dr. M. Kawamura and the Fujisawa Pharmaceutical Co., Ltd., Japan, for the gift of **1**, Dr. T. Platt (University of Rochester) for the overproducing strain of rho, and Dr. A. Tripathy of UNC's Macromolecular Interactions Facility for help in the isothermal calorimetry experiments.

SUPPORTING INFORMATION AVAILABLE

Simulated kinetic profiles for the poly(C)-dependent kinetics for reactions using 16−256 μM $MgCl_2$ and 2−2560 μM ATP. This information is available free of charge via the Internet at http://pubs.acs.org.

REFERENCES

1. Roberts, J. W. (1969) Termination factor for RNA synthesis, *Nature 224*, 1169−1174.
2. Richardson, J. P., and Greenblatt, J. (1996) in *Escherichia coli and Salmonella typhimurium: Cellular and Molecular Biology* (Neidhardt, F. C., et al., Eds.) pp 822−848, American Society for Microbiology, Washington, DC.
3. Richardson, J. P. (1991) Preventing the synthesis of unused transcripts by rho factor, *Cell 64*, 1047−1049.
4. (a) Richardson, J. P. (1990) Rho-dependent transcription termination, *Biochim. Biophys. Acta 1048*, 127−138; (b) Platt, T., and Richardson, J. P. (1992) in *Transcriptional Regulation* (McKnight, S. L., and Yamamoto, K. R., Eds.) pp 365−388, Cold Spring Harbor Laboratory Press, Plainview, NY.
5. Pinkham, J. L., and Platt, T. (1983) The nucleotide sequence of the *rho* gene of *E. coli* K-12, *Nucleic Acids Res. 11*, 3531−3545.
6. Briercheck, D. M., Wood, T. C., Allison, T. J., Richardson, J. P., and Rule, G. S. (1998) The NMR structure of the RNA binding domain of *E. coli* rho factor suggests possible RNA-protein interactions, *Nat. Struct. Biol. 5*, 393−399.
7. Allison, T. J., Wood, T. C., Briercheck, D. M., Rastinejad, F., Richardson, J. P., and Rule, G. S. (1998) Crystal structure of the RNA-binding domain from transcription termination factor rho, *Nat. Struct. Biol. 5*, 352−356.
8. Richardson, J. P. (1996) Structural organization of transcription termination factor Rho, *J. Biol. Chem. 271*, 1251−1254.
9. Horiguchi, T., Miwa, Y., and Shigesada, K. (1997) The quaternary geometry of transcription termination factor rho: Assignment by chemical cross-linking, *J. Mol. Biol. 269*, 514−528.
10. Miwa, Y., Horiguchi, T., and Shigesada, K. (1995) Structural and functional dissections of transcription termination factor Rho by random mutagenesis, *J. Mol. Biol. 254*, 815−837.
11. Magyar, A., Zhang, X., Abdi, F., Kohn, H., and Widger, W. R. (1999) Identifying the bicyclomycin binding domain through biochemical analysis of antibiotic-resistant rho proteins, *J. Biol. Chem. 274*, 7316−7324.
12. Vincent, F., Openshaw, M., Trautwein, M., Gaskell, S. J., Kohn, H., and Widger, W. R. (2000) Rho transcription factor: Symmetry and binding of bicyclomycin, *Biochemistry 39*, 9077−9083.

13. Zwiefka, A., Kohn, H., and Widger, W. R. (1993) Transcription termination factor rho: The site of bicyclomycin inhibition in *Escherichia coli*, *Biochemistry 32*, 3564−3570.
14. Magyar, A., Zhang, X., Kohn, H., and Widger, W. R. (1996) The antibiotic bicyclomycin affects the secondary RNA binding site of *Escherichia coli* transcription termination factor Rho, *J. Biol. Chem. 271*, 25369−25374.
15. Vincent, F., Srinivasan, J., Santillán, A., Jr., Widger, W. R., and Kohn, H. (2001) C(5)−C(5a)-Modified bicyclomycins: Synthesis, structure, and biochemical and biological properties, *J. Org. Chem. 66*, 2251−2264.
16. Weber, J., Nadanaciva, S., and Senior, A. E. (2000) ATP-driven rotation of the γ subunit in F_1-ATPase, *FEBS Lett. 483*, 1−5.
17. (a) Dombroski, A. J., Brennan, C. A., Spear, P., and Platt, T. (1988) Site-directed alterations in the ATP-binding domain of rho protein affect its activities as a termination factor, *J. Biol. Chem. 263*, 18802−18809; (b) Walstrom, K. M., Dozono, J. M., and von Hippel, P. H. (1998) Effects of reaction conditions on RNA secondary structure and on the helicase activity of *Escherichia coli* transcription termination factor rho, *J. Mol. Biol. 279*, 713−726; (c) Stitt, B. L. (1988) *Escherichia coli* transcription termination protein rho has three hydrolytic sites for ATP, *J. Biol. Chem. 263*, 11130−11137.
18. (a) Lowery, C., and Richardson, J. P. (1977) Characterization of the nucleoside triphosphate phosphohydrolase (ATPase) activity of RNA synthesis termination factor ρ. I. Enzymatic properties and effects of inhibitors, *J. Biol. Chem. 252*, 1375−1380; (b) Faus, I., and Richardson, J. P. (1989) Thermodynamic and enzymological characterization of the interaction between transcription termination factor ρ and λ cro mRNA, *Biochemistry 28*, 3510−3517; (c) Brennan, C. A., Steinmetz, E. J., Spear, P., and Platt, T. (1990) Specificity and efficiency of rho-factor helicase activity depends on magnesium concentration and energy coupling to NTP hydrolysis, *J. Biol. Chem. 265*, 5440−5447.
19. Mott, J. E., Grant, R. A., Ho, Y.-S., and Platt, T. (1985) Maximizing gene expression from plasmid vectors containing the λP_L promoter: Strategies for overproducing transcription termination factor ρ, *Proc. Natl. Acad. Sci. U.S.A. 82*, 88−92.
20. Nehrke, K. W., Seifried, S. E., and Platt, T. (1992) Overproduced rho factor from p39AS has lysine replacing glutamic acid at residue 155 in the linker region between its RNA and ATP binding domains, *Nucleic Acids Res. 20*, 6107.
21. Lowry, O. H., Rosebrough, N. J., Farr, A. L., and Randall, R. J. (1951) Protein measurement with the folin phenol reagent, *J. Biol. Chem. 193*, 265−275.
22. Wu, A. M., Christie, G. E., and Platt, T. (1981) Tandem termination sites in the tryptophan operon of *Escherichia coli*, *Proc. Natl. Acad. Sci. U.S.A. 78*, 2913−2917.
23. Sharp, J. A., Galloway, J. L., and Platt, T. (1983) A kinetic mechanism for the poly(C)-dependent ATPase of the *Escherichia coli* transcription termination protein, rho, *J. Biol. Chem. 258*, 3482−3486.
24. Wiseman, T., Williston, S., Brandts, J. F., and Lin, L. N. (1989) Rapid measurement of binding constants and heats of binding using a new titration calorimeter, *Anal. Biochem. 179*, 131−137.
25. For similar observations, see refs *17c* and *18a*.
26. (a) Segel, I. H. (1975) A is a nonessential activator; Only SA binds to the catalytic site, in *Enzyme Kinetics*, pp 267−270, John Wiley & Sons, New York; (b) London, W. P., and Steck, T. L. (1969) Kinetics of enzyme reactions with interaction between a substrate and a (metal) modifier, *Biochemistry 8*, 1767−1779.
27. For similar values, see refs *17a* and *18a*; (a) Seifried, S. E., Wang, Y., and von Hippel, P. H. (1988) Fluorescent modification of the cysteine 202 residue of *Escherichia coli* transcription termination factor rho, *J. Biol. Chem. 263*, 13511−13514; (b) Park, H.-g., Zhang, X., Moon, H.-s., Zwiefka, A., Cox, K., Gaskell, S. J., Widger, W. R., and Kohn, H. (1995) Bicyclomycin and dihydrobicyclomycin inhibition kinetics of *Escherichia coli* rho-dependent transcription termination factor ATPase activity, *Arch. Biochem. Biophys. 323*, 447−454.
28. Khan, M. M. T., and Martell, A. E. (1966) Thermodynamic quantities associated with the interaction of adenosine triphosphate with metal ions, *J. Am. Chem. Soc. 88*, 668−671.
29. Richardson, J. P., and Macy, M. R. (1981) Ribonucleic acid synthesis termination protein ρ function: effects of conditions that destablize ribonucleic acid secondary structure, *Biochemistry 20*, 1133−1139.
30. Smith, R. A., Latchney, L. R., and Senior, A. E. (1985) Tight divalent metal binding to *Escherichia coli* F_1-adenosinetriphosphatase. Complete substitution of intrinisic magnesium by manganese or cobalt and studies of metal binding sites, *Biochemistry 24*, 4490−4494.
31. Guex, N., and Peitsch, M. C. (1997) SWISS-MODEL and the Swiss-Pdb Viewer: An environment for comparative protein modeling, *Electrophoresis 18*, 2714−2723.
32. Xu, Y., Kohn, H., and Widger, W. R. (2002) Mutations in rho transcription termination factor that affect RNA tracking, *J. Biol. Chem. 277*, 30023−30030.
33. (a) Wei, R. R., and Richardson, J. P. (2001) Identification of an RNA-binding site in the ATP-binding domain of *Escherichia coli* by H_2O_2/Fe-EDTA cleavage protection studies, *J. Biol. Chem. 276*, 28380−28387; (b) Wei, R. R., and Richardson, J. P. (2001) Mutational changes of conserved residues in the Q-loop region of transcription factor rho greatly reduce secondary site RNA-binding, *J. Mol. Biol. 314*, 1007−1015.
34. Moyse, K. A., Knight, J. S., and Richardson, J. P. (2000) The bicyclomycin sensitivities of 38 bicyclomycin-resistant mutants of transcription termination protein rho and the location of their mutations support a structural model of rho based on the F_1 ATPase, *J. Mol. Biol. 302*, 565−579.
35. Dombroski, A. J., LaDine, J. R., Cross, R. L., and Platt, T. (1988) The ATP binding site on rho protein, *J. Biol. Chem. 263*, 18810−18815.

BI020420W